Research Journal of Applied Sciences, Engineering and Technology 4(12): 1672-1676, 2012
ISSN: 2040-7467

Submitted: November 10, 2011 Accepted: November 29, 2011 Published: June 15, 2012

1D Modeling of a Bifacial Silicon Solar Cell under Frequency Modulation Monochromatic Illumination: Determination of the Equivalent Electrical Circuit Related to the Surface Recombination Velocity

[1]H. Ly Diallo, [2]M. Wade, [2]I. Ly, [3]M. NDiaye, [4]B. Dieng, [5]O.H. Lemrabott, [6]A.S. Maïga and [3]G. Sissoko
[1]University of Thies, UFR/SET, Thies, Senegal
[2]Ecole Polytechnique of Thies, EPT, Thies, Senegal
[3]Faculty of Science and Technology, University Cheikh Anta Diop, Dakar, Senegal
[4]University of Bambey, UFR SATIC, UBI, Physics Section, Bambey, Senegal
[5]Higher Multinational School of Telecommunications, ESMT, Dakar, Senegal
[6]University Gaston Berger, UFR/SAT, Applied Physics Section, Saint Louis, Senegal

Abstract: We present in this study the determination of the equivalent electrical circuits associated to the recombination velocities for a bifacial silicon solar cell under frequency modulation and monochromatic illumination. This determination is based on Bode and Nyquist diagrams that is the variations of the phase and the module of the back surface and intrinsic junction recombination velocities. Their dependence on illumination wavelength is also shown.

Key words: Bode diagram, electrical circuit, recombination velocities, solar cell

INTRODUCTION

The improvement of solar cells performance needs quality control in all steps of the cells manufacturing. Since solar cells quality is strongly dependent on microscopic (Mazhari and Morkoç, 1993) and electrical parameters (Anil Kumar and Martinuzzi, 1989) many characterization methods where developedin steady state as well as in transient state and frequency modulation for their control during cells manufacturing.

In this study, we propose a method for the determination of equivalent electrical models associated to recombination velocities in a bifacial silicon solar cell under frequency modulation and monochromatic illumination. These models will be deduced from the Bode diagram (Anil Kumar *et al*., 2001; Dieng *et al*., 2007) of the recombination velocities.

THEORETICAL MODEL

We consider a n^+- p - p^+ polycrystalline silicon with back surface field presented on Fig. 1

In this study, we neglect the emitter contribution and consider a quasi-neutral base. When the solar cell is illuminated in frequency modulation, the excess minority carriers generated in the base of the solar cell obey the following continuity equation:

$$D.\frac{\partial^2 \delta_3(x,t)}{\partial x^2} - \frac{\delta_3(x,t)}{\tau} = -G_3(x,t) + \frac{\partial \delta_3(x,t)}{\partial t} \quad (1)$$

$\delta_3(x, t)$ and $G_3(x, t)$ are respectively excess minority carriers density and generation rate at position x and time t. We have:

$$\delta_3(x,t) = \delta_3(x)\exp(i\omega t) \quad (2)$$

and

$$G_3(x,t) = g_3(x)\exp(i\omega t) \quad (3)$$

$\delta_3(x)$ and $g_3(x)$ are related to position x and exp(iwt) related to time t:

$$g_3(x) = \alpha I_0(1-R)\left[e^{-\alpha x} + e^{(-\alpha(H-x))}\right] \quad (4)$$

with: $\alpha(\lambda)$ is the absoption coefficient at wavelength λ ; $R(\lambda)$ is the reflexion coefficient at wavelength λ; H is the base width,

D is the diffusion coefficient and t is the minority carrier lifetime.

We have:

Corresponding Author: Gregoire Sissoko, Faculty of Science and Technology, University Cheikh Anta Diop, Dakar, Senegal

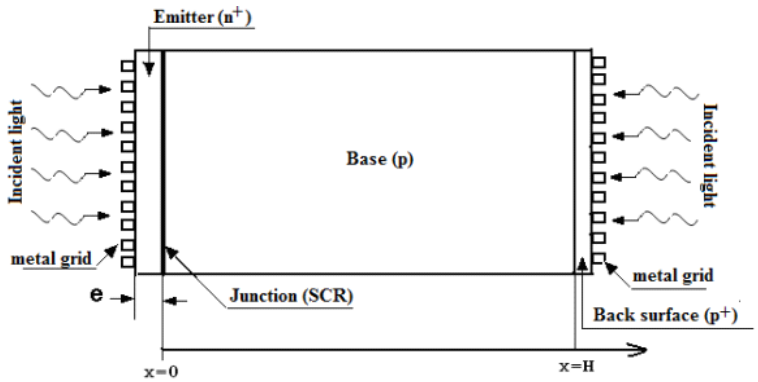

Fig. 1: Bifacial n+-p-p+ silicon solar cell

$$L^2 = \tau D$$

$$\frac{1}{L(\omega)^2} = \frac{1}{L^2} \times (i\omega\tau + 1)$$

were L(ω) is the complex diffusion length. Replacing Eq. (2), (3), (4) into Eq. (1), we obtain:

$$\frac{\partial^2 \delta_3(x)}{\partial x^2} - \frac{1}{L(\omega)^2}.\delta_3(x) = -\frac{g_3(x)}{D} \quad (5)$$

The general solution of Eq. (5) is in the form:

$$\delta_3(x) = A_3 \cosh\left(\frac{x}{L}\right) + B_3 \sinh\left(\frac{x}{L}\right) - \frac{\alpha I_0.(1-R)L^2.(e^{-\alpha x} + e^{(-\alpha(H-x))})}{D.(\alpha^2.L^2 - 1)} \quad (6)$$

Coefficients A_3 and B_3 are to be determined by use of the following boundary conditions:

- At the junction (x = 0):

$$\frac{\partial \delta_3(x)}{\partial x}\Big|_{x=0} = \frac{Sf_3}{D}\delta_3(0) \quad (7)$$

- At the back surface (x = H):

$$\frac{\partial \delta_3(x)}{\partial x}\Big|_{x=H} = -\frac{Sb_3}{D}\delta_3(H) \quad (8)$$

Sf_3 and Sb_3 are respectively junction and back surface recombination velocities.

Photocurrent density profile: Applying Fick's law, we have:

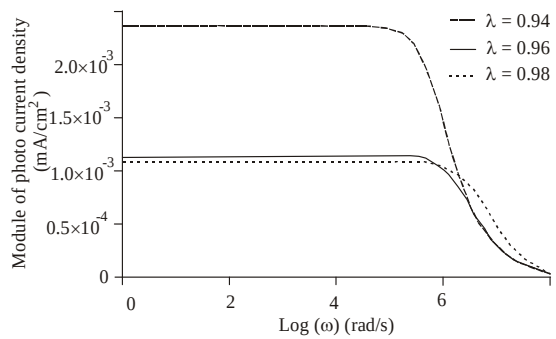

Fig. 2: Photocurrent density module versus modulation frequency for various wavelengths

$$J_3(\lambda, \omega, Sf_3, Sb_3) = q.D.\frac{\partial \delta_3(x, \lambda, \omega, Sf_3, Sb_3)}{\partial x}\Big|_{x=0} \quad (9)$$

q is the elementary charge.

We present on Fig. 2 the photocurrent density versus modulation frequency for various wavelengths.

The photocurrent didn't varie with frequency in the range [0 Hz; 4.10^4 rad/s]; that is a quasi-steady state, then the photocurrent decreases until 6.10^6 were it vanishes completely. Very high frequencies freeze the relaxation process in the solar cell. The photocurrent seems to be inverslyproportionnal to the wavelength if the wavelength is greater than à 0.8 µm.

Back surface recombination velocity profile: The back surface recombination is determined by use of the following equation (Chenvidhya *et al*., 2003):

$$\frac{\partial J_3(\lambda, \omega, Sf_3, Sb_3)}{\partial Sf_3} = 0 \quad (10)$$

Solving Eq. (10) leads to:

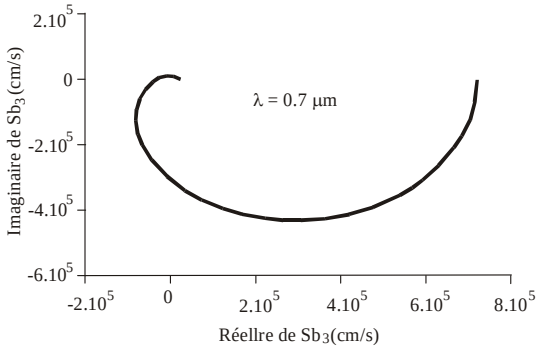

(a)

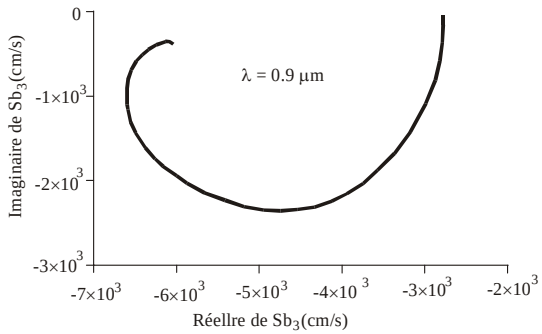

(b)

Fig. 3: Nyquist diagram of the back surface recombination velocity for various wavelengths L = 0.02cm, H = 0.03cm ; D = 26cm^2/s

$$Sb_3 = D.\frac{\left[\begin{array}{l} L(\omega).\alpha\left\{1+\cosh\left(\frac{H}{L(\omega)}\right)\right\} \\ +\sinh\left(\frac{H}{L(\omega)}\right)\end{array}\right].e^{-\alpha.H} - L(\omega).\alpha.\left[\begin{array}{l}1+\cosh\left(\frac{H}{L(\omega)}\right)\\ +\sinh\left(\frac{H}{L(\omega)}\right)\end{array}\right]}{L(\omega)\left[\begin{array}{l}1-\cosh\left(\frac{H}{L(\omega)}\right)-L(\omega)\\ .\alpha.\sinh\left(\frac{H}{L(\omega)}\right)\end{array}\right].e^{-\alpha.H} + L(\omega)\left[\begin{array}{l}1-\cosh\left(\frac{H}{L(\omega)}\right)+L(\omega)\\ .\alpha.\sinh\left(\frac{H}{L(\omega)}\right)\end{array}\right]} \quad (11)$$

Rewriting Eq. (11) give us:

$$Sb_3(\omega,\lambda) = \left[F(\omega,\lambda) + iG(\omega,\lambda)\right] = \left|Sb_3(\omega,\lambda)\right|e^{i\phi Sb3(\omega)} \quad (12)$$

We present the Nyquist diagram of the back surface recombination velocity on Fig. 3 for various wavelengths.

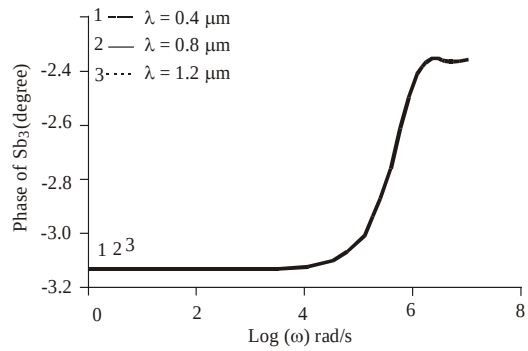

Fig. 4: Bode diagram of the back surface recombination velocity for various wavelengths: the phase L= 0.02 cm; H = 0.03 cm; D = 26 cm^2/s

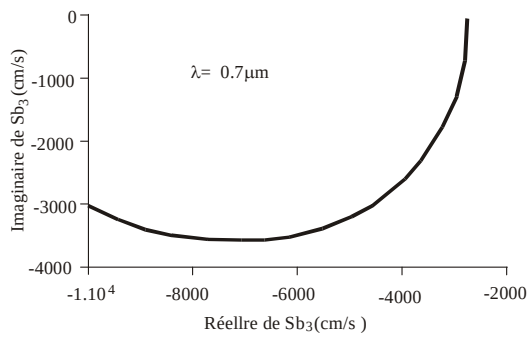

(a)

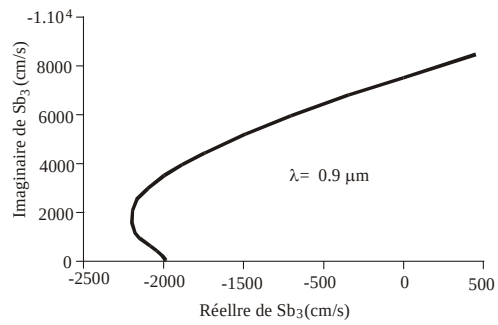

(b)

Fig. 5: Nyquist diagram of the intrinsic junction recombination velocity for various wavelengths L = 0.02 cm, H = 0.03 cm, D = 26 cm^2/s

The representation of the imaginary part according to the real part the recombination velocity at the rear is a semi-circle which shows the capacitive effects of recombination rate

We present now the Bode diagram of the back surface recombination velocity (phase) on Fig. 4.

This figure shows that the phase is constant for low frequencies, whatever the wavelength: it is the quasi steady-state. For high frequencies, the phase increases but

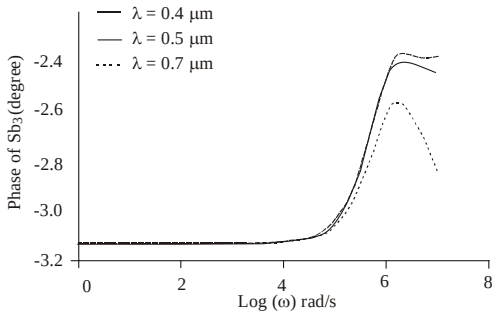

Fig. 6: Bode diagramm of the intrinsic junction recombination velocity for various wavelengths: the phase (a). L = 0.02 cm; H = 0.03 cm; D = 26 cm^2/s

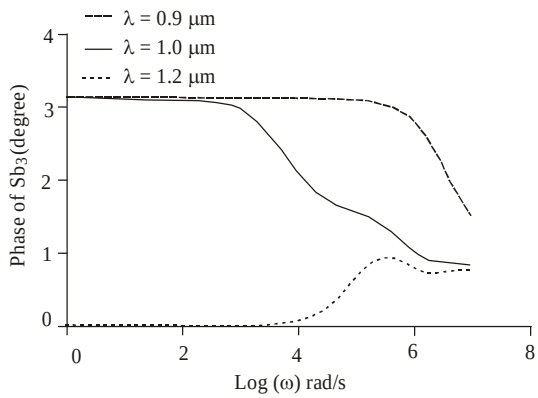

Fig. 7: Bode diagram of the intrinsic junction recombination velocity for various wavelengths: the phase (b). L = 0.02 cm; H = 0.03 cm; D = 26 cm^2/s

remains negative. The back surface recombination effects are capacitive type.

Intrinsic junction recombination velocity profile: We use the following equation to determine the intrinsic junction recombination velocity:

$$\frac{\partial J_3(\lambda,\omega,Sf_3,Sf_3)}{\partial Sb_3} = 0 \tag{13}$$

Solving Eq. (13) leads to:

$$Sf\,0_3 = D.\frac{\left[\sinh\left\{\frac{H}{L(\omega)}\right\}.\left[e^{-\alpha.H}+1\right]-\alpha.L(\omega)\right]}{L(\omega).\left[\alpha.L(\omega).\left[1-e^{-\alpha.H}\right].sosh\left(\left\{\frac{H}{L(\omega)}\right\}+\left[1+e^{-\alpha.H}\right].\left[1-\cosh\left(\frac{H}{L(\omega)}\right)\right]\right)\right]} \tag{14}$$

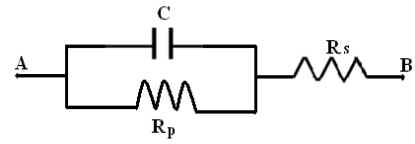

Fig. 8: Equivalent electrical circuit for back surface recombination velocity

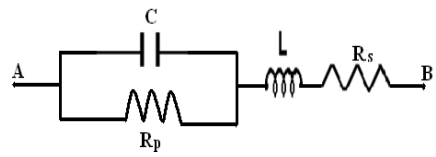

Fig. 9: Equivalent electrical circuit for intrinsic junction recombination velocity

Nyquist diagram of the intrinsic junction recombination velocity is presented on Fig. 5 for various wavelengths.

The representation of the imaginary part according to the real part the intrinsic rate of recombination at the junction shows the effects of inductive and capacitive the rate of recombination.

We present now the Bode diagram (phase) of intrinsic junction recombination velocity.

Figure 6 show that for frequency less than 0.8 μm, the phase is negative with increasing part after a certain frequency limit. The losses are capacitive type.

For frequency greater than 0.8 μm, the phase is presented on Fig. 7.

The phase of the intrinsic junction recombination for this range of frequency stays positive; that is the losses are of inductive type.

EQUIVALENT ELECTRICAL CIRCUITS

Bode representations of recombination velocities show that:

- The phase for back surface recombination velocity is always negative
- The corresponding losses are of capacitive type This leads us to conclude that these losses could be represented by the following equivalent electrical circuit (Dieng *et al*., 2011: Sissoko *et al*., 1996).

This circuit characterize the capacitive phenomenon observed on Fig. 8; C is the equivalent capacitance, Rp the parallel resistance associated to the leakage current and Rs the series resistance associated to the ohmic losses due to maerial resistivity and electrical contacts.

For the intrinsic junction recombination, the phase is positive for a given wavelength and negative elsewhere; this traduce a capacitive type and inductive typebehavior

depending on the wavelength.The associated equivalent circuit is presented in Fig. 9.

This circuit traduces the inductive and capacitive behavior observed on Fig. 6 and 7 trough inductance L, Capacitance C, parallel resistance Rp and series resistance Rs.

CONCLUSION

A method to determine the equivalent electrical circuit associated to recombination velocities in a bifacial solar cell has been presented. The cell is under frequency modulation and monochromatic illumination. This method is based on the Bode and Nyquist diagrams for various wavelengths and has been applied for simultaneous front and back sides illumination.

REFERENCES

Anil Kumar, H. and S. Martinuzzi, 1989. Influence of dislocations on electrical properties of large grained polycrystalline silicon cells. II. Experimental results. J. Appl. Phys., 66(4): 1717-1726.

Anil Kumar, R., M.S. Suresh and J. Nagaraju, 2001. Measurement of AC parameters of gallium arsenide (GaAs/Ge) Solar Cell by impedance spectroscopy. IEE Trans. Electron Devices, 48(9): 2177-2179.

Chenvidhya, D., K. Kirtikara and C. Jivacate, 2003. Study of a PV-grid connected system on its output harmonics solarenergy. Mater. Solar Cells, 8: 459-464.

Dieng, A., L. OuldHabiboulahy, A.S. Maiga, A. Diao and G. Sissoko, 2007. Impedance spectroscopymethod applied to electrical parameters determination on bifacial dilicon solar cell under magnetic field. J. Des Sci.,7(3): 48-52.

Dieng, A., N. Thiam, A. Thiam, A.S. Maiga and G. Sissoko, 2011. Magnetic field effect on the electrical parameters of a polycrystalline silicon solar cell. Res. J. Appl. Sci. Eng. Technol., 3(7): 602-611.

Mazhari, B. and H. Morkoç, 1993. Surface recombination in GaAs PN junction diode J. Appl. Phys., 73(11): 7509-7514.

Sissoko, G., C. Museruka, A. Corréa, I. Gaye and A.L. Ndiaye, 1996. Ligth spectral essect an recombination parameters as silicon solar cell. World Renew. Energ. Cong. Art, 3: 1487-1490.